Astron. Astrophys. 339, 225–238 (1998)

ASTRONOMY
AND
ASTROPHYSICS

The effect of delays on filament oscillations and stability

G.H.J. van den Oord, N.A.J. Schutgens, and M. Kuperus

Sterrekundig Instituut, Utrecht University, P.O. Box 80.000, 3508 TA Utrecht, The Netherlands

Received 21 April 1998 / Accepted 17 July 1998

Abstract. We discuss the linear response of a filament to perturbations, taking the finite communication time between the filament and the photosphere into account. The finite communication time introduces delays in the system. Recently Schutgens (1997ab) investigated the solutions of the delay equation for vertical perturbations. In this paper we expand his analysis by considering also horizontal and coupled oscillations. The latter occur in asymmetric coronal fields. We also discuss the effect of Alfvén wave emission on filament oscillations and show that wave emission is important for stabilizing filaments. We introduce a fairly straightforward method to study the solutions of delay equations as a function of the filament–photosphere communication time. A solution can be described by a linear combination of damped harmonic oscillations each characterized by a frequency, a damping/growth time and, accordingly, a quality factor. As a secondary result of our analysis we show that, within the context of line current models, Kippenhahn/Schlüter-type filament equilibria can never be stable in the horizontal and the vertical direction at the same time but we also demonstrate that Kuperus/Raadu-type equilibria can account for both an inverse or a normal polarity signature. The diagnostic value of our analysis for determining, e.g., the filament current from observations of oscillating filaments is discussed.

Key words: Sun: filaments – Sun: prominences – Sun: magnetic fields – Sun: oscillations – MHD – waves

1. Introduction

In two recent papers Schutgens (1997ab) considered the effect of the finite Alfvén velocity on the vertical stability of a filament and on its fundamental mode of oscillation. It was found that a finite Alfvén velocity introduces delays in a system and changes its stability properties.

The plasma contained in filaments is supported against gravity by the Lorentz force. This implies that a current runs in the filament body. The field related to this filament current can only penetrate slowly in the photosphere because of the induced inertial currents caused by the rapid increase of the density towards the photosphere which acts as a rigid wall. As a result the filament field is shielded by a photospheric surface current distribution. In fact, the photospheric surface can be considered as a separatrix surface over which the tangential component of the filament field jumps to zero. Kuperus & Raadu (1974) showed that this surface current can be represented by a virtual (mirror) current distribution below the photosphere, analogous to the method of images in electrostatics.

Changes in the filament position introduce changes in the surrounding magnetic field. These take a finite time to reach the photospheric boundary where they induce changes in the surface current distribution. From any point on the surface it then takes again a finite time to propagate the information about the changes in the surface current to the filament. The finite communication time thus introduces delays in the system. Schutgens analyzed the effect of these delays on the response of a filament to vertical perturbations. In this paper we expand his analyses in three ways: 1) we discuss, next to vertical oscillations, the cases of horizontal and coupled oscillations, 2) we investigate the effect of damping by the emission of Alfvén waves, and 3) we propose a new method to determine the oscillation frequencies and damping times as a function of the communication time between the filament and the photosphere.

Delay studies require information about the stability properties of a filament in the quasi-static approach, in which delays are ignored because of the implicit assumption that the Alfvén velocity is infinite. Therefore we discuss in the first part of the paper various filament equilibria and their stability properties based on this approach (Sects. 2 and 3). In Sect. 4 we derive the linearized delay equations for the general case of coupled horizontal and vertical oscillations. For filaments in symmetric coronal background fields these equations decouple into independent equations for horizontal and vertical oscillations.We also introduce a new method of solution which is illustrated using a simplified delay equation. In Sect. 5 we discuss the response to vertical and horizontal perturbations in the absence of a damping mechanism. The effect of damping due to the emission of Alfvén waves by an oscillating filament is discussed in Sect. 6 for vertical, horizontal and coupled oscillations. Our conclusions are presented in Sect. 7.

Send offprint requests to: G.H.J. van den Oord

2. Quasi-stationary approach

Consider a filament suspended in a coronal background magnetic field $\boldsymbol{B}_{\rm cor}$. The axial filament current I runs in the x-direction. The filament is at a height z_0 above the photosphere. At a depth $-z_0$ below the photosphere there is a (virtual) mirror current of strength $-I$ whose related magnetic field is indicated as $\boldsymbol{B}_{\rm mir}$. The components of the momentum equation of the filament are given by

$$m\frac{d^2y}{dt^2} \;=\; -\frac{I}{c}\left(B_{\rm z,mir}+B_{\rm z,cor}\right)\,, \tag{1}$$

$$m\frac{d^2z}{dt^2} \;=\; \frac{I}{c}\left(B_{\rm y,mir}+B_{\rm y,cor}\right)-mg\,, \tag{2}$$

where m is the mass per unit length of the filament and g is the gravitational acceleration

$$g=\frac{GM_\odot}{\left(R_\odot+z_0\right)^2}>0\,.$$

The role of the mirror current is to guarantee that the field related to the filament current cannot penetrate the photosphere. This requires that the positions of the filament current and the mirror current are always symmetric with respect to the photospheric plane. The sum of the fields of the filament current and the mirror current then has no component normal to the photosphere. A consequence of this symmetry is that the field related to the mirror current has no z-component at the location of the filament so that in Eq. (1) $B_{\rm z,mir}=0$. Force equilibrium in horizontal direction then implies that the filament can only be located at positions where $B_{\rm z,cor}=0$. Force equilibrium in vertical direction implies that the right-hand side of Eq. (2) equals zero. This results in a quadratic equation for the filament equilibrium current I_0 (see van Tend & Kuperus 1978)

$$\left(\frac{I_0}{c}\right)^2\frac{1}{z_0}+\left(\frac{I_0}{c}\right)B_{\rm y,cor}-mg=0\,, \tag{3}$$

which has two possible solutions

$$\left(\frac{I_0}{c}\right)=-\frac{1}{2}z_0B_{\rm y,cor}\pm\frac{1}{2}z_0\sqrt{B_{\rm y,cor}^2+4mg/z_0}\,. \tag{4}$$

These can be related to Kippenhahn/Schlüter (KS, Kippenhahn & Schlüter 1957) and Kuperus/Raadu (KR, Kuperus & Raadu 1974) equilibria. A KS equilibrium is characterized by the fact that the Lorentz force by the mirror current can be neglected in the force balance. The upward Lorentz force by the coronal background field balances the downward gravitational acceleration. In a KR equilibrium gravity is not important in the force balance so that the upward Lorentz force by the mirror current is balanced by the downward Lorentz force of the coronal background field. These equilibria follow naturally from Eq. (4) when $z_0B_{\rm y,cor}^2\gg 4mg$ and a Taylor expansion for the square root is used. The 'minus' solution is $(I_0/c)\approx -z_0B_{\rm y,cor}$ which corresponds to a KR equilibrium. The 'plus' solution gives $(I_0/c)B_{\rm y,cor}\approx mg$ so a KS equilibrium.

When the coronal background field is bipolar a KR equilibrium is classified as Inverse Polarity (IP) and a KS equilibrium as Normal Polarity (NP). NP means that the direction of the transverse field, as measured in the filament, has the same direction as the direction expected from a bipolar photospheric polarity distribution. For IP equilibria these directions are opposite (see, e.g., Fig. 2 in Schutgens 1997b).

The linear stability of the system follows from applying small displacements δy and δz to the equilibrium. An important constraint is that during the perturbation the filament field must not penetrate the photosphere (flux conservation). This implies that during the displacement the mirror current must be displaced in accordance with the filament so that the positions of the displaced filament current and the mirror current remain symmetric with respect to the photosphere. Therefore $B_{\rm z,mir}$ remains zero at the location of the displaced filament and the mirror current does not provide a horizontal force component on the filament. Linearizing Eqs. (1) and (2) then gives

$$m\delta\ddot{y} \;=\; -\frac{I_0}{c}\left.\frac{\partial B_{\rm z,cor}}{\partial y}\right|_{\rm E}\delta y-\frac{I_0}{c}\left.\frac{\partial B_{\rm z,cor}}{\partial z}\right|_{\rm E}\delta z\,,$$

$$\begin{aligned} m\delta\ddot{z} \;=\; &\left(-\frac{I_0^2}{c^2}\frac{1}{z_0^2}+\frac{I_0}{c}\left.\frac{\partial B_{\rm y,cor}}{\partial z}\right|_{\rm E}-m\left.\frac{\partial g}{\partial z}\right|_{\rm E}\right)\delta z\\ &+\frac{I_0}{c}\left.\frac{\partial B_{\rm y,cor}}{\partial y}\right|_{\rm E}\delta y\,, \end{aligned}$$

with index 'E' indicating the equilibrium position. The last terms on the right-hand side of these expressions show that, in principle, the horizontal and vertical response to perturbations are coupled. In a system with translation symmetry in the x-direction it follows from $\boldsymbol{\nabla}\cdot\boldsymbol{B}_{\rm cor}=0$ that $\partial B_{\rm y,cor}/\partial y|_{\rm E}=-\,\partial B_{\rm z,cor}/\partial z|_{\rm E}$ so that the coupling constants have the same magnitude. The horizontal and vertical response decouple for a filament on the axis of symmetry of a symmetric background field. In that case the equations can be written as $\delta\ddot{y}+\Omega_{\rm y}^2\delta y=0$ and $\delta\ddot{z}+\Omega_{\rm z}^2\delta z=0$ with

$$\Omega_{\rm y}^2 \;\equiv\; \frac{1}{m}\frac{I_0}{c}\left.\frac{\partial B_{\rm z,cor}}{\partial y}\right|_{\rm E} \tag{5}$$

and

$$\Omega_{\rm z}^2 \;\equiv\; \frac{1}{m}\left(\frac{I_0^2}{c^2}\frac{1}{z_0^2}-\frac{I_0}{c}\left.\frac{\partial B_{\rm y,cor}}{\partial z}\right|_{\rm E}+m\left.\frac{\partial g}{\partial z}\right|_{\rm E}\right) \tag{6}$$

the quasi-stationary oscillation frequencies for oscillations in the horizontal and vertical direction, respectively. When $\Omega_{\rm y}^2$ or $\Omega_{\rm z}^2$ is negative the system is unstable.

3. Stability of filament equilibria

In this section we discuss the horizontal and vertical stability of KS and KR equilibria for various types of coronal background fields. We call a specific filament equilibrium stable when both $\Omega_{\rm y}^2>0$ and $\Omega_{\rm z}^2>0$.

3.1. Filaments in potential fields

In a potential field it follows from $\boldsymbol{\nabla}\times\boldsymbol{B}_{\rm cor}=\boldsymbol{0}$ that $\partial B_{\rm z,cor}/\partial y=\partial B_{\rm y,cor}/\partial z$. This identity provides a relation between Eqs. (5) and (6) which we use below.

For a KS equilibrium we found in Sect. 2 that the equilibrium current is given by $I_0/c \approx mg/B_{\rm y,cor}$. This gives for $\Omega_{\rm y}^2$ and $\Omega_{\rm z}^2$

$$\Omega_{\rm y}^2 \approx \frac{g}{B_{\rm y,cor}}\frac{\partial B_{\rm y,cor}}{\partial z}\,, \tag{7}$$

$$\Omega_{\rm z}^2 \approx -g\left(\frac{1}{B_{\rm y,cor}}\frac{\partial B_{\rm y,cor}}{\partial z}+\frac{2}{R_\odot+z_0}-\frac{1}{z_0}\frac{mg}{z_0 B_{\rm y,cor}^2}\right) \tag{8}$$

$$\approx -\frac{g}{B_{\rm y,cor}}\frac{\partial B_{\rm y,cor}}{\partial z}\,. \tag{9}$$

These expressions are valid for a sufficiently strong field at the location of the filament ($z_0 B_{\rm y,cor}^2 \gg 4mg$). The expressions show that for a KS equilibrium $\Omega_{\rm y}^2 \approx -\Omega_{\rm z}^2$ so that these quantities can never be positive at the same time. Therefore stable KS equilibria do not exist. We note that a filament can be located in a (∪-shaped) dip of the coronal field or at (∩-shaped) crest (e.g., at the apex of an arcade-like field). A dip is characterized by $(1/B_{\rm y,cor})(\partial B_{\rm y,cor}/\partial z)$ being positive while at a crest this product is negative (this statement holds independent of the direction of $B_{\rm y,cor}$). So a KS equilibrium requires a dip for horizontal stability and a crest for vertical stability. These requirements are incompatible. Van Tend & Kuperus (1978) already noted that KS prominences are horizontally unstable when located at a crest. Here we find that a dip indeed stabilizes the filament in horizontal direction but destabilizes it in vertical direction.

For KR equilibria the equilibrium current is given by $(I_0/c) \approx -z_0 B_{\rm y,cor}$ while gravity can be neglected. In that case we have

$$\Omega_{\rm y}^2 \approx -\frac{z_0 B_{\rm y,cor}}{m}\frac{\partial B_{\rm y,cor}}{\partial z}\,, \tag{10}$$

$$\Omega_{\rm z}^2 \approx \frac{1}{m}\left(B_{\rm y,cor}^2 + z_0 B_{\rm y,cor}\frac{\partial B_{\rm y,cor}}{\partial z}\right)\,. \tag{11}$$

Horizontal stability requires the presence of a crest in the coronal field at the location of the filament. Vertical stability is guaranteed as long as the height of the filament (z_0) is smaller than the the typical scale height of the field (for further discussion on the vertical stability see van Tend & Kuperus 1978).

Above we considered the limit $B_{\rm y,cor}^2 \gg 4mg/z_0$. In the opposite limit, which applies to (locally) very weak coronal fields, Eq. (4) gives for the equilibrium current $(I_0/c) \approx \pm\sqrt{mgz_0}$. In this limit there is mainly a balance between the Lorentz force by the mirror current and gravity. Because the current can be of either sign, horizontal stability can always be realized. For vertical perturbations we find

$$\Omega_{\rm z}^2 \approx \frac{g}{z_0}\left(\frac{R_\odot - z_0}{R_\odot + z_0}\right) - \Omega_{\rm y}^2\,.$$

Provided $\Omega_{\rm y}^2$ is sufficiently small this expression indicates that the filament is stable in vertical direction up to approximately a solar radius. The reason for this stability is that for filament heights up to a solar radius the gravitational acceleration can be considered to be constant while the mirror force varies proportional to $1/z_0$. These conditions are favourable to drive a filament back to its equilibrium after a perturbation. At larger heights the gravitational acceleration drops faster than the mirror force so that there is no restoring force after a perturbation. This type of 'weak field' equilibrium (WF hereafter) applies to very heavy filaments or filaments in regions with weak coronal fields like, e.g., found outside active regions or close to X-type neutral lines in the coronal field.

3.2. Parameters for delay studies

In Sects. 5 and 6 we discuss the effects of delays for various filament equilibria. In this section we calculate a number of parameters which are used in those sections. We consider a filament located in an asymmetric background field which is the sum of a potential arcade and a constant field in the z-direction. The components of the coronal field are then given by $B_{\rm y,cor} = -B_0\cos ky\mathrm{e}^{-kz}$ and $B_{\rm z,cor} = B_0\sin ky\mathrm{e}^{-kz} - B_1$ ($B_1 > 0$). Force equilibrium in the horizontal direction requires that $\sin ky_0\mathrm{e}^{-kz_0} = B_1/B_0 \equiv \epsilon$. In the following we use dimensionless quantities defined by $I = cz_0B_0I'$, $B = B_0B'$, $z = z_0z'$, $y = z_0y'$, $\chi = kz_0$, $\rho = \sqrt{1-\epsilon^2\mathrm{e}^{2\chi}}$ ($\rho = \cos ky_0$), $\kappa = 2z_0/(R_\odot + z_0)$, $t = (\sqrt{m}/B_0)t'$ and $g = (z_0B_0^2/m)g'$. The value of the dimensionless gravitational acceleration g' is a small number of the order $2.7\,10^{-5}(m/10^6)(g/g_\odot)(z_0/10^9)^{-1}(B_0/10^3)^{-2}$. Of course, for weak photospheric fields g' can become of the order unity. Eq. (4) can be written as (we drop the accents)

$$I_0 = \frac{1}{2}\rho\mathrm{e}^{-\chi} \pm \frac{1}{2}\left(\rho^2\mathrm{e}^{-2\chi}+4g\right)^{1/2}\,. \tag{12}$$

In this expression we have taken the equilibrium height of the filament equal to z_0 so that $z' = 1$. The dimensionless currents and frequencies associated with the KR, KS and WF solutions are given by

	KR ($g \ll 1$)	KS ($g \ll 1$)	WF ($g \gg 1$)
I_0:	$\rho\mathrm{e}^{-\chi}$	$-g\mathrm{e}^{\chi}/\rho$	$\sqrt{g}$
$\Omega_{\rm z}^2$:	$\rho^2(1-\chi)\mathrm{e}^{-2\chi}$	$(\chi-\kappa)g$	$g(1-\kappa)-\Omega_{\rm y}^2$
$\Omega_{\rm y}^2$:	$\rho^2\chi\mathrm{e}^{-2\chi}$	$-\chi g$	$\rho\sqrt{g}\chi\mathrm{e}^{-\chi}$
$\tilde\Omega_{\rm z}^2$:	$(1-\chi)$	$\rho^2(\chi-\kappa)\mathrm{e}^{-2\chi}/g$	$(1-\kappa)-\Omega_{\rm y}^2/g$
$\tilde\Omega_{\rm y}^2$:	χ	$-\rho^2\chi\mathrm{e}^{-2\chi}/g$	$\rho\chi\mathrm{e}^{-\chi}/\sqrt{g}$

The case of a filament in a symmetric background field is recovered by taking $B_1 = 0$ which corresponds to $\epsilon = 0$ and $\rho = 1$. The expressions show that KS prominences are unstable to horizontal perturbations because $\Omega_{\rm y}^2 < 0$. KR prominences are stable for perturbations in the horizontal direction and become unstable in the vertical direction at heights $\chi > 1$.

The dimensionless quantities $\tilde\Omega_{\rm z}^2 \equiv \Omega_{\rm z}^2/I_0^2$ and $\tilde\Omega_{\rm y}^2 \equiv \Omega_{\rm y}^2/I_0^2$ play an important role in the study of delay equations. These quantities can be interpreted as the ratio of the inertia of an oscillating filament and the Lorentz force due to the mirror current. The inertial term in the momentum equation can be approximated as $md^2z/dt^2 \approx mz_0\Omega^2$ so that the ratio is given by $mz_0^2\Omega^2/(I_0/c)^2$. In dimensionless units this corresponds to $\tilde\Omega^2$.

Stability requires that $\tilde{\Omega}_{\rm z}^2 > 0$ and $\tilde{\Omega}_{\rm y}^2 > 0$. On the other hand we see from the expressions above that for KR prominences $\tilde{\Omega}_{\rm y}^2 + \tilde{\Omega}_{\rm z}^2 = 1$. This implies that for stable KR prominences $\tilde{\Omega}_{\rm z}^2$ and $\tilde{\Omega}_{\rm y}^2$ always have values between zero and unity. WF equilibria satisfy $\tilde{\Omega}_{\rm y}^2 + \tilde{\Omega}_{\rm z}^2 \lesssim 1 - \kappa$.

3.3. Filaments in force-free background fields

Suppose that a filament is embedded in a force-free field with translation symmetry in the x-direction. From the x-component of Ampère's law it follows that $\partial B_{\rm z,cor}/\partial y - \partial B_{\rm y,cor}/\partial z = \alpha B_{\rm x,cor}$ with α the force-free parameter. The expressions for $\boldsymbol{B}_{\rm cor}$ can be found in, e.g., Amari & Aly (1989). An analysis, similar to that in the previous section, shows that KS equilibria are horizontally unstable in force-free arcades. The reason is, of course, that the filament is located at a crest in the field. For the other types of equilibrium we find (dimensionless)

$$\tilde{\Omega}_{\rm y}^2 + \tilde{\Omega}_{\rm z}^2 \approx \begin{cases} 1 + \alpha'^2/\gamma & \text{KR}\,, \\ 1 - \kappa & \text{WF}\,, \end{cases}$$

with $\alpha' = \alpha z_0$ and $\gamma = \sqrt{\chi^2 - \alpha'^2}$. These expressions show that, as expected, the properties of the WF equilibrium do not differ from the potential case (for which $\alpha' = 0$). For KR equilibria in force-free arcades $\tilde{\Omega}_{\rm y}^2 + \tilde{\Omega}_{\rm z}^2$ does becomes larger than unity but only significantly when $\alpha' \to \chi$. There exist, however, various problems when one tries to model a line current in a force-free field. These are discussed in Sect. 7.

3.4. KS versus KR and NP versus IP

Our results indicate that KS equilibria cannot exist in potential fields because they are unstable in either the horizontal or vertical direction. This is a serious disadvantage of the KS model when compared with the KR model. Within the context of line current models for filament equilibria the KR model has several additional advantages over the KS model. First of all, in a KR model the filament current runs at the natural location of a neutral line of the (combined) mirror and background field. Secondly, the appearance of a KR equilibrium shows more resemblance with real filaments than KS equilibria. The reason is that the filament mass will accumulate at those positions where the magnetic field has a dip. In KR models the field possesses dips over a considerable range of heights below the filament current giving the filament a slab-like appearance, as observed. KS equilibria possess only a small dip (see, e.g., Fig. 2 in Schutgens 1997b) making a slab-like appearance impossible. An implication is that in KR equilibria the filament current and the (partly) neutral filament mass are spatially separated making Ohmic losses unimportant. In KS equilibria the filament current and the location of the dip are (almost) co-spatial so that the current can be susceptible to collisional losses. This is undesirable given the long life times of filament.

From an observational point of view it is impossible to distinguish between a KS and a KR filament because observations do not provide enough information to estimate the magnitudes of the terms in the (vertical) force balance. However, it can be argued that in a bipolar coronal field a KS filament has a NP topology and a KR filament an IP. This then can be used to classify filaments as KS or KR based on the NP/IP classification which can be determined from observations. The problem is that we demonstrated that KS-type filaments can not exist which makes it difficult to explain the observed NP topologies. A way out is to put a KR filament in a quadrupolar field. We show below that a KR filament in a quadrupolar field can account for both an IP and a NP signature. As an example we consider two cases where the coronal background field results from two sub-photospheric line dipoles. In one case these are horizontally displaced and of equal strength and direction (see Fig. 1a for the resulting field topology). Possible filament locations are on the symmetry axis of the configuration. In the second case we place one line dipole below the other and let the line dipoles have different strengths and opposite directions (see Fig. 1f). The figures show that in both quadrupolar field configurations there is a neutral point. The horizontal field component below the neutral point is opposite to the horizontal field component above the neutral point. For a large range of (relative) strengths of the line dipoles and filament masses we solved Eq. (4) and selected those solutions which are stable ($\Omega_{\rm y}^2 > 0$ and $\Omega_{\rm z}^2 > 0$). Almost all stable solutions turned out to be KR type so with the Lorentz force of the background field pointing downward. In addition there exists a narrow range of equilibrium heights around the neutral point for which the force balance is mainly between the mirror force and gravity (so a WF equilibrium). The small contribution to the force balance by the locally weak coronal field is in upward direction when the filament current is located just below the neutral point and in downward direction for the filament current located just above the neutral point.

In Figs. 1b and 1g we show the field topology when we place a filament below the neutral point which exists in the background field. Figs. 1c and 1h show the field near the filament in more detail. The thick vertical lines indicate the locations where mass can be stored in dips in the field. The arrows indicate the direction of the field as it would be measured. The plus and minus signs indicate the polarity of the photospheric field. The small arrows below the photosphere indicate the expected field direction when an observer uses the photospheric polarities adjacent to the filament. The large arrows indicate the expected field direction if the observer bases his/her estimate on the dominant photospheric field distribution. In Figs. 1d and 1i we show the field topology when the filament is above the neutral point in the background field (Figs. 1e and 1j show again enlargements). Comparing Figs. 1c and 1e, and Figs. 1h and 1i, shows that the direction of the field in the filament changes as a function of height. Independent of whether an observer uses the small scale or large scale photospheric field distribution, one filament will be classified as NP and the other as IP although all equilibria shown are of the KR type. This can possibly explain our result that KS equilibria cannot exist while still accounting for the fact that both IP and NP configurations are observed. For the whole parameter range we investigated we found for the KR equilibria that $\tilde{\Omega}_{\rm y}^2 + \tilde{\Omega}_{\rm z}^2 \lesssim 1$.

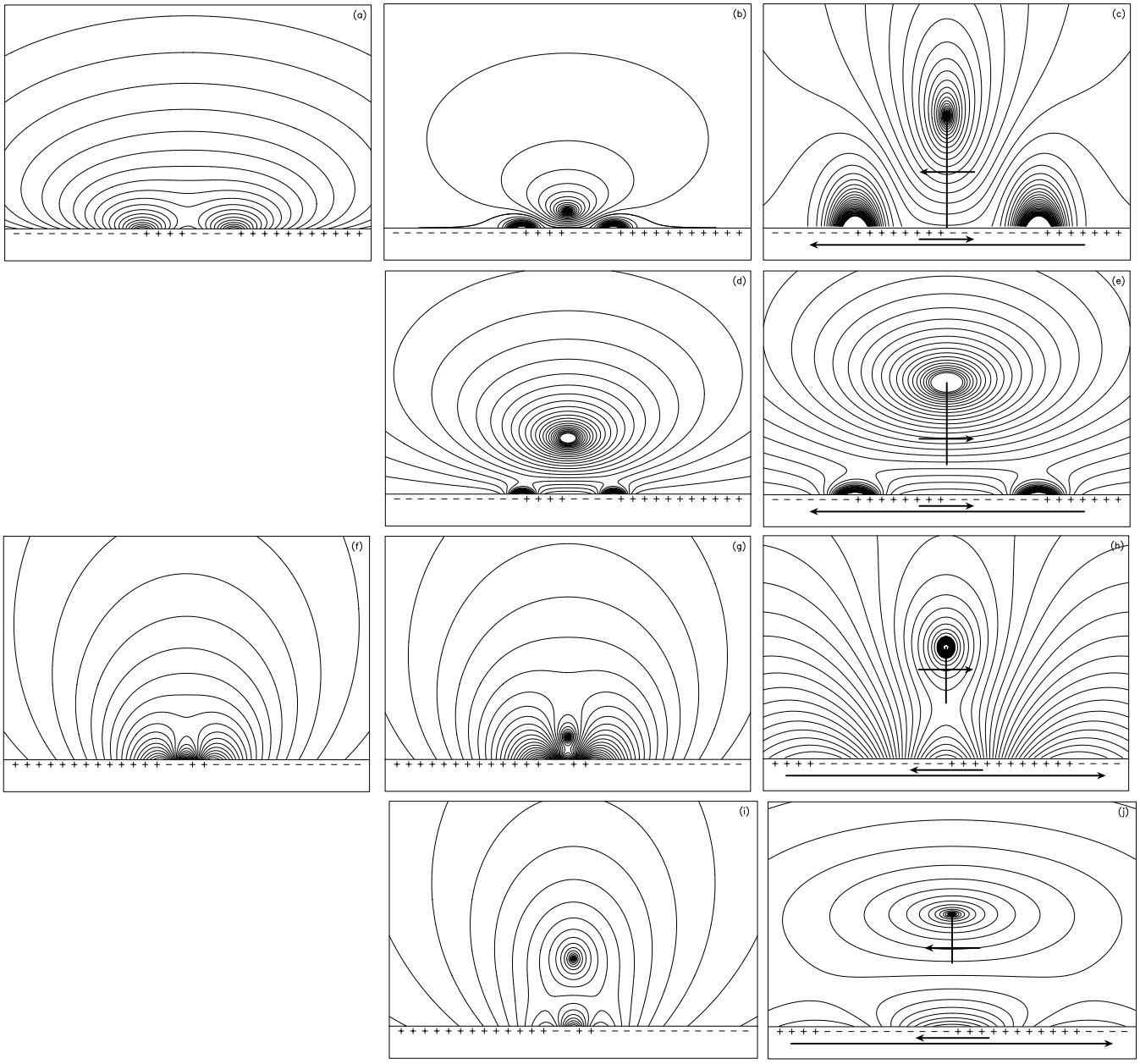

Fig. 1a–j. Filament equilibria in quadrupolar background fields created by two sub-photospheric line dipoles. In panels **a**-**e** the line dipoles have the same depth, strength and orientation but are horizontally separated over a distance of ten times their depth. In panels **f**-**j** the line dipoles are vertically displaced: the upper line dipole points to the right while the lower points to the left and is twice as strong. The ratio of the depths of the line dipoles equals two. Panels **a** and **f** show the coronal background field which has a neutral point below the dips in the field lines. In panels **b** and **g** we place a filament below this neutral point and in panels **d** and **i** above it. Panels **c**, **e**, **h** and **j** are enlargements of the field near the filament. The plus and minus signs indicate the photospheric polarity distribution. The thick vertical line indicates locations where mass can be stored in field lines with dips. The arrow indicate the direction of the field in the filament. The arrows at the bottom of the panels indicate the expected direction of the field in the filament based on the photospheric polarities: the small arrow for the case that an observer uses the photospheric polarities adjacent to the filament and the large arrows when the large scale photospheric polarity distribution is used. The configurations in panels **b** and **d** apply to, e.g., a filament between two active regions.

4. Linearized delay equations

In Eqs. (1) and (2) the evolution of $\boldsymbol{B}_{\rm mir}$ reflects in reality the evolution of the photospheric surface current. Since changes in $\boldsymbol{B}_{\rm mir}$ propagate with the coronal Alfvén velocity, the characteristic time scale is given by $\tau = 2z_0/v_{\rm A}$ where z_0 is the height of the filament and $v_{\rm A}$ is the Alfvén velocity. The appropriate expressions for $\boldsymbol{B}_{\rm mir}$, taking the finite communication time into account, are derived following the method outlined in Schutgens

(1997a) resulting in

$$B_{\rm y,mir}(y(t),z(t)) = \frac{2I_0}{c}\times \qquad (13)$$
$$\int_0^\infty dx' \left(\frac{1}{v_{\rm A}RF}\right)^2 \left\{ v_{\rm A}\dot{z}(t') + \frac{z(t)+z(t')}{RF}(v_{\rm A}^2+\dot{G})\right\},$$

$$B_{\rm z,mir}(y(t),z(t)) = \frac{2I_0}{c}\times \qquad (14)$$
$$\int_0^\infty dx' \left(\frac{1}{v_{\rm A}RF}\right)^2 \left\{ v_{\rm A}\dot{y}(t') - \frac{y(t)-y(t')}{RF}(v_{\rm A}^2+\dot{G})\right\},$$

with $R(t') = \sqrt{x'^2+(y(t)-y(t'))^2+(z(t)+z(t'))^2}$, $F = 1+(1/v_{\rm A})\partial R(t')/\partial t'$ and $\dot{G} = -\dot{y}(t')^2+(y(t)-y(t'))\ddot{y}(t')-\dot{z}(t')^2-(z(t)+z(t'))\ddot{z}(t')$. The dimensionless delay time is (we drop the accent)

$$\tau = \frac{B_0}{\sqrt{m}}\frac{2z_0}{v_{\rm A}} = 8\frac{z_0}{d}\left(\frac{\rho_{\rm cor}}{\rho_{\rm fil}}\right)^{1/2} \approx 0.25\frac{z_0}{d}\left(\frac{10^3\rho_{\rm cor}}{\rho_{\rm fil}}\right)^{1/2}$$

where d is the diameter of a filament with a circular cross-section and $\rho_{\rm cor}$ and $\rho_{\rm fil}$ are the mass densities in the corona and the filament, respectively. In general the dimensionless delay time will be of the order unity.

Linearizing Eqs. (1), (2),(13) and (14), and taking the Laplace transform of the results gives two characteristic equations (see Appendix A). Define $Z(s) \equiv \mathcal{L}(\delta z(t))$ and $Y(s) \equiv \mathcal{L}(\delta y(t))$. The characteristic equations are given by (dimensionless form)

$$Zv(s) - YI_0 \left.\frac{\partial B_{\rm y,cor}}{\partial y}\right|_{\rm E} = 0\,, \qquad (15)$$

$$Yh(s) + ZI_0 \left.\frac{\partial B_{\rm z,cor}}{\partial z}\right|_{\rm E} = 0\,, \qquad (16)$$

with

$$v(s) = s^2 + \Omega_{\rm z}^2 - \frac{1}{2}I_0^2\left(1+\tau^2 s^2 K_1'(\tau s)\right)\,, \qquad (17)$$

$$h(s) = s^2 + \Omega_{\rm y}^2 - \frac{1}{2}I_0^2\left(1-\tau s K_1(\tau s)\right)\,. \qquad (18)$$

In these expression $K_{\rm n}$ is the modified Bessel function of the second kind of order n. A prime indicates a differentiation with respect to the argument of the Bessel function. The complex variable s can be written as $s = \nu + i\omega$. Eqs. (15) and (16) are, in principle, coupled but for a filament in a symmetric background field they decouple and the characteristic equations become $v(s) = 0$ and $h(s) = 0$. In that case the horizontal and vertical response are independent. Vertical oscillations have been studied in Schutgens (1997b).

The properties of characteristic equations are discussed in Schutgens (1997a). Solutions of a characteristic equation occur in complex conjugate pairs and therefore correspond to a response function of the form $\exp(\nu t)\sin(\omega t)/\omega$. So when the real part (ν) of s is positive the system is unstable. When ν is negative, the system is damped and when $\nu = 0$ the system performs marginally stable oscillations with frequency ω. In the limit $\tau = 0$, the characteristic equations for (decoupled) vertical and horizontal oscillations become $s^2 = -\Omega_{\rm z}^2$ and $s^2 = -\Omega_{\rm y}^2$, respectively, and the quasi-stationary case is recovered. When $\tau \neq 0$ a characteristic equation possesses an infinite number of solutions, referred to as poles (in the complex plane). There is at most a finite number of poles with $\nu > \alpha$ for α an arbitrary real number. The evolution of the system is mainly determined by those poles which have the largest value of ν. Note that the location of a pole in the complex plane can be directly related to the quality factor ($Q = \omega/2\nu$) of the corresponding mode of oscillation. The delay time τ appears as a control parameter in the characteristic equations. For $\tau = 0$ only the quasi-stationary poles are found in the complex (ν,$i\omega$) plane. When τ becomes slightly different from zero these quasi-stationary poles start to move in the complex plane and at the same time an infinite number of poles appears at large negative values of ν. When τ is varied all poles move in a continuous way through the complex plane. Instability requires that there is at least one pole in the real positive half-space $\nu > 0$ of the complex plane. Poles can only enter that half-space by crossing the imaginary axis. This property of the solutions is used in the following to study the stability of filaments and to determine the trajectories of poles as a function of τ.

There is an advantage to rewrite Eqs. (17) and (18) using the following scaling: $s = \tilde{s}|I_0|$, $\tau = \tilde{\tau}/|I_0|$, $\Omega_{\rm z}^2 = \tilde{\Omega}_{\rm z}^2 I_0^2$ and $\Omega_{\rm y}^2 = \tilde{\Omega}_{\rm y}^2 I_0^2$. The equations then become

$$v(\tilde{s}) = \tilde{s}^2 + \tilde{\Omega}_{\rm z}^2 - \frac{1}{2}\left(1+\tilde{\tau}^2\tilde{s}^2 K_1'(\tilde{\tau}\tilde{s})\right) \qquad (19)$$

$$h(\tilde{s}) = \tilde{s}^2 + \tilde{\Omega}_{\rm y}^2 - \frac{1}{2}\left(1-\tilde{\tau}\tilde{s}K_1(\tilde{\tau}\tilde{s})\right) \qquad (20)$$

In this form the imaginary parts do not explicitly depend on the characteristic parameters of a specific filament equilibrium. These are contained in $\Omega_{\rm y,z}^2$ and I_0^2 (or $\tilde{\Omega}_{\rm y,z}^2$).

Solving Eqs. (19) and (20) is rather complicated because of the appearance of the Bessel functions. Also we have, in principle, to determine an infinite number of poles. These poles can be located graphically in the complex plane ($\tilde{\nu}$,$i\tilde{\omega}$) by considering the real and imaginary parts of the above expressions and by using a contour algorithm to plot the zero contours of these parts for a given value of $\tilde{\tau}$. The poles are found at the intersections of the real and imaginary zero contours. For a presentation in a paper this method is not suitable because there are simply too many zero contours, often very close to each other. However, we are primarily interested in determining that value of τ for which a system becomes unstable. Therefore we discuss in the following a simplified characteristic equation with the aim to illustrate the method of analysis we use in Sect. 5 to solve Eqs. (19) and (20). The poles of this simplified equation have approximately the same typical behaviour as those of Eqs. (19) and (20). For a different method of solution we refer to Schutgens (1997a).

A simplified characteristic equation can be derived by including a factor $2\delta(x')$ (delta function) in the integrands of the linearized expression for $B_{\rm y,mir}$ (Eq. (A1)). The resulting linearized expression for δz is

$$\delta\ddot{z}(t) + \frac{\tau^2 I_0^2}{4}\delta\ddot{z}(t-\tau) + \frac{\tau I_0^2}{2}\delta\dot{z}(t-\tau)$$

$$+\left(\Omega_{\rm z}^2-\frac{I_0^2}{2}\right)\delta z(t)+\frac{I_0^2}{2}\delta z(t-\tau)=0\,.$$

Note that in the quasi-stationary approach ($\tau=0$) this expression reduces to $\delta\ddot{z}(t)+\Omega_{\rm z}^2\delta z(t)=0$, as expected. Taking the Laplace transform gives the characteristic equation $e(s)$ of our example

$$e(\tilde{s})=\tilde{s}^2+\tilde{\Omega}_{\rm z}^2-\frac{1}{2}+{\rm e}^{-\tilde{\tau}\tilde{s}}\left\{\frac{1}{2}+\frac{1}{2}\tilde{\tau}\tilde{s}+\frac{1}{4}\tilde{\tau}^2\tilde{s}^2\right\}\,.$$

For $\tilde{\tau}=0$ we find a pair of quasi-stationary poles at $\tilde{s}=\pm i\tilde{\Omega}_{\rm z}$. When $\tilde{\tau}$ increases these two poles move in the complex plane while at the same time an infinite number of poles is found in the negative real half-space of the complex plane. The latter poles correspond to damped oscillations. It is interesting to see for which values of $\tilde{\tau}$ these poles arrive on the imaginary axis ($\tilde{s}=i\tilde{\omega}$). In that case we have

$$\begin{aligned}e(i\tilde{\omega}) \;=\; & -\tilde{\omega}^2+\tilde{\Omega}_{\rm z}^2\\ & -\frac{1}{2}+\cos(\tilde{\omega}\tilde{\tau})\left(\frac{1}{2}-\frac{1}{4}\tilde{\omega}^2\tilde{\tau}^2\right)+\frac{1}{2}\tilde{\omega}\tilde{\tau}\sin(\tilde{\omega}\tilde{\tau})\\ & +i\left\{\frac{1}{2}\tilde{\omega}\tilde{\tau}\cos(\tilde{\omega}\tilde{\tau})-\left(\frac{1}{2}-\frac{1}{4}\tilde{\omega}^2\tilde{\tau}^2\right)\sin(\tilde{\omega}\tilde{\tau})\right\}\,.\end{aligned}$$

Write $u=\tilde{\omega}\tilde{\tau}$, then the condition ${\rm Im}(e(i\tilde{\omega}))=0$ can be written as $\tan u=2u/(2-u^2)$. The solutions of this equation form a sequence $u_{\rm k}$ given by $u_0=0$, $u_1=0.66\pi$, $u_2=1.89\pi$, $u_3=2.93\pi$, $u_4=3.94\pi\ldots u_{\rm k}\to{\rm k}\pi-2/({\rm k}\pi)$. Not all solutions $u_{\rm k}$ are also solutions to the real part of the characteristic equation. Only those which result in $\tilde{\omega}^2>0$ correspond to true intersections with the imaginary axis. The value of $\tilde{\omega}^2$ depends of course on the values of $\tilde{\Omega}_{\rm z}^2$. In Sect. 3 we showed that $\tilde{\Omega}_{\rm z}^2\lesssim 1$. This implies that $\tilde{\omega}^2>0$ only occurs for ${\rm k}=0$ and all odd values of k. For each of these values of k we can determine the corresponding frequency $\tilde{\omega}_{\rm k}$ and the delay time at which the pole is on the imaginary axis $\tilde{\tau}_{\rm k}=u_{\rm k}/\tilde{\omega}_{\rm k}$. As an example we take $\tilde{\Omega}_{\rm z}^2=0.5$ then $\tilde{\omega}_0=\tilde{\Omega}_{\rm z}=\sqrt{0.5}$ at $\tilde{\tau}_0=0$, $\tilde{\omega}_1=1.09$ at $\tilde{\tau}_1=1.91$, etcetera. For larger (odd) values of k we have that $\tilde{\omega}_{\rm k}\approx{\rm k}\pi/2$ and $\tilde{\tau}_{\rm k}\to 2$. This implies that all poles with k larger than, say, 3 intersect the imaginary axis at approximately the same delay time $\tilde{\tau}$.

Next we establish in which direction a pole moves when it intersects the imaginary axis. Suppose that $e(\tilde{s})=0$ for a given pole $\tilde{s}_{\rm k}$. We consider small variations of $\tilde{\tau}$ under the constraint $de=0$:

$$de=\frac{\partial e}{\partial\tilde{s}}d\tilde{s}+\frac{\partial e}{\partial\tilde{\tau}}d\tilde{\tau}=0\,.$$

The direction in which a pole moves is then given by

$$\frac{d\tilde{s}}{d\tilde{\tau}}=-\left.\frac{\partial e/\partial\tilde{\tau}}{\partial e/\partial\tilde{s}}\right|_{\tilde{s}_{\rm k},\tilde{\tau}}\equiv-\dot{S}\,,\qquad(21)$$

and the system of differential equations which governs the behaviour of a pole in the complex plane is given by

$$\frac{d\tilde{\nu}}{d\tilde{\tau}}=-{\rm Re}(\dot{S})\;\;\text{and}\;\;\frac{d\tilde{\omega}}{d\tilde{\tau}}=-{\rm Im}(\dot{S})\,.\qquad(22)$$

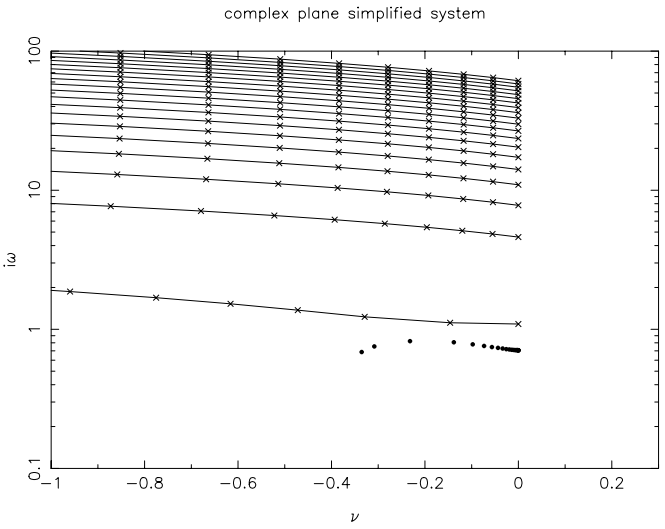

Fig. 2. Behaviour of the poles in the complex plane for $\tilde{\Omega}_{\rm z}^2=0.5$. The dots indicate the trajectory of the quasi-stationary pole which moves to the left. At the same time other poles approach from the left. The lines indicate the trajectories of some of these poles (from bottom to top ${\rm k}=1,3,5,\ldots,39$). Each trajectory ends when a pole is exactly on the imaginary axis at the corresponding value of $\tilde{\tau}$ for that pole. The ${\rm k}=1$ pole arrives on the imaginary axis at $\tilde{\tau}=1.09$, all the other poles at $1.99<\tilde{\tau}<2$. The increment between the dots and the crosses, respectively, is $\Delta\tilde{\tau}=0.1$.

These expressions imply that the direction in which a pole on the imaginary axis moves is given by $-{\rm sign}({\rm Re}(\dot{S}))$. For our example we find that this direction is given by ${\rm sign}(-u_{\rm k}^2\cos(u_{\rm k}))$. If this quantity is positive the pole moves to the right and when it is negative the pole moves to the left. It can easily be checked that all poles with odd k move to the right so towards the unstable part of the complex plane. For the quasi-stationary pole we have $u_0=0$ and our expression shows that the pole does not move in the $\tilde{\nu}$ direction at $\tilde{\tau}_0=0$. In order to find the direction into which the pole moves at some small but finite delay time $\tilde{\tau}=\epsilon$ we can use ${\rm sign}(-\tilde{\Omega}_{\rm z}^2\epsilon^2\cos(\tilde{\omega}_{\rm z}\epsilon))$ with $\epsilon\ll 1$. This implies that the quasi-stationary pole will move to the left for small values of $\tilde{\tau}$ and the system performs damped oscillations.

In Fig. 2 we show the behaviour of the poles in the complex plane. The thick dots locate the trajectory of the stationary pole ($\tilde{\omega}_0=\sqrt{0.5}$) which moves to the left. The trajectory is shown for $0\le\tilde{\tau}\le 2$ and the increment between two dots is $\Delta\tilde{\tau}=0.1$. The lines indicate the trajectories of the poles $u_{\rm k}$ (${\rm k}=1,3,5,\ldots,39$) with increments $\Delta\tilde{\tau}=0.1$ indicated by the crosses. These poles move to the right and the trajectories end on the right-hand side at the delay time $\tilde{\tau}$ at which each of the poles intersects the imaginary axis. The quality factor ($Q=\tilde{\omega}/2|\tilde{\nu}|=\omega/2|\nu|$) of the oscillations of the quasi-stationary pole follows from the position of this pole in the complex plane.

In summary, an investigation of the solutions of a characteristic equation consists of the following steps: 1) consider the poles on the imaginary axis; 2) determine the solutions $\tilde{\omega}\tilde{\tau}$ of the imaginary part of the characteristic equation; 3) check, using the

real part of the characteristic equation, which of the combinations $\tilde{\omega}\tilde{\tau}$ result in $\tilde{\omega}^2 \geq 0$; 4) determine the delay time at which the pole is on the imaginary axis from $\tilde{\omega}$ and $\tilde{\omega}\tilde{\tau}$; 5) determine the direction in which each of the poles moves. This then selects the range of $\tilde{\tau}$ over which stable solutions are found. If required, the trajectories of the poles can be found by (backward or forward) integration of Eq. (21) using the position on the imaginary axis and the corresponding delay time as initial conditions. The evaluation of $\dot{S}$ often results in lengthy expressions. In this paper we usually present only that part of the specific expression which determines the sign of $\mathrm{Re}(\dot{S})$.

5. Solutions to the delay equations

In this section we discuss the behaviour of the poles of Eqs. (19) and (20) for a filament embedded in a potential field. The behaviour of the poles is discussed along the lines of our example in Sect. 4.

5.1. Vertical oscillations

Consider the case of vertical oscillations. When there is a pole on the imaginary axis ($\tilde{s} = i\tilde{\omega}$) Eq. (19) can be written as

$$v(i\tilde{\omega}) \;=\; -\tilde{\omega}^2 + \tilde{\Omega}_{\rm z}^2 - \frac{1}{2} + \frac{\pi}{4}\tilde{\omega}^2\tilde{\tau}^2 Y_1'(\tilde{\omega}\tilde{\tau}) + \frac{\pi}{4} i\tilde{\omega}^2\tilde{\tau}^2 J_1'(\tilde{\omega}\tilde{\tau})\;,$$

with $J_{\rm n}$ and $Y_{\rm n}$ Bessel functions of order n of the first and second kind respectively. The condition $\mathrm{Im}(v(i\tilde{\omega})) = 0$ is satisfied when $\tilde{\omega}\tilde{\tau} = 0$ or $J_1'(\tilde{\omega}\tilde{\tau}) = 0$. The case $\tilde{\omega}\tilde{\tau} = 0$ corresponds to the quasi-stationary case ($\tau = 0$). The zeros of J_1' are given by $j'_{1;{\rm k}}$ with the index k denoting the number of the zero (see Abramowitz & Stegun 1968). For simplicity we label the (quasi-stationary) zero $\tilde{\omega}\tilde{\tau} = 0$ as ${\rm k} = 0$ and use ${\rm k} \geq 1$ for the series $j'_{1;{\rm k}}$.

The direction in which the poles move is given by Eq. (21). After some lengthy algebra it can be shown that $\mathrm{sign}(\mathrm{Re}(d\tilde{s}/d\tilde{\tau})) \sim \mathrm{sign}((j'^2_{1;{\rm k}}-1)J_0(j'_{1;{\rm k}})) \sim \mathrm{sign}(J_1(j'_{1;{\rm k}}))$. This implies that all poles with odd values of k move to the right and those with even k to the left. The pole which is present on the imaginary axis for $\tilde{\tau} = 0$ first moves to the left when $\tilde{\tau}$ starts to differ from zero.

The corresponding values of $\tilde{\omega}^2$ follow from $\mathrm{Re}(v(i\tilde{\omega})) = 0$. We write the latter expression as $\tilde{\omega}^2 = \tilde{\Omega}_{\rm z}^2 - f(j'_{1;{\rm k}})$ with $f(j'_{1;{\rm k}}) \equiv \frac{1}{2}\left\{1 - \frac{\pi}{2} j'^2_{1;{\rm k}} Y_1'(j'_{1;{\rm k}})\right\}$. In Table 1 we give the first six zeros and the values of the function $f(j'_{1;{\rm k}})$.

To discuss the behaviour of the poles in the complex plane we recall that stability of the quasi-stationary equilibrium of a filament in a potential background field implies $0 < \tilde{\Omega}_{\rm z}^2 \lesssim 1$. For this range of values $\tilde{\Omega}_{\rm z}^2$ can take, all $j'_{1;{\rm k}}$ with $f(j'_{1;{\rm k}}) > 0$ result in $\tilde{\omega}^2 < 0$. Therefore only the ${\rm k} = 0$ pole and the poles with odd k represent valid solutions. Table 1 shows that when τ starts to differ from zero, the pole which is present on the imaginary axis starts to move into the negative real half-space of the complex plane so that the filament starts to perform damped oscillations.

Table 1. The first six zeros and the values of the functions $f(j'_{1;{\rm k}})$ and $g(j_{1;k})$ at these zeros. Note that $j'_{1,0}$ is not a true zero of J_1' but is a solution of $\mathrm{Im}(v(i\tilde{\omega})) = 0$. The arrows indicate whether the pole moves to the right or to the left when τ is increased.

k	$j'_{1;{\rm k}}$	$f(j'_{1;{\rm k}})$		$j_{1;{\rm k}}$	$g(j_{1;k})$	
0	0.00	0.00	$\leftarrow$	0.00	0.00	$\rightarrow$
1	1.84	-1.08	$\rightarrow$	3.83	1.74	$\leftarrow$
2	5.33	8.20	$\leftarrow$	7.02	-1.17	$\rightarrow$
3	8.54	-15.11	$\rightarrow$	10.17	2.50	$\leftarrow$
4	11.71	25.59	$\leftarrow$	13.32	-1.79	$\rightarrow$
5	14.86	-35.40	$\rightarrow$	16.47	3.05	$\leftarrow$

As τ is increased further there is again a pole on the imaginary axis when $\tilde{\omega}\tilde{\tau} = 1.84$. This occurs when $\tilde{\omega}^2 = \tilde{\Omega}_{\rm z}^2 + 1.08$ and $\tilde{\tau} = 1.84/\sqrt{\tilde{\Omega}_{\rm z}^2 + 1.08}$. For larger values of $\tilde{\tau}$ the pole moves into that part of the complex plane where the filament is unstable. For even larger values of $\tilde{\tau}$ more poles cross the imaginary axis into the unstable part of the complex plane. From this we conclude that vertically stable or damped solutions are only possible for $0 \leq \tilde{\tau} \leq 1.84/\sqrt{\tilde{\Omega}_{\rm z}^2 + 1.08}$. This corresponds to the parameter range investigated by Schutgens (1997ab). In his study of forced oscillations Schutgens (1997b, see his Fig. 9) found that the response function has a maximum near $\Omega_{\rm z}\tau = 1$. This point is located near the instability strip. Our analysis shows that this maximum corresponds to the presence of a pole on the imaginary axis at $\omega\tau = 1.84$ (${\rm k} = 1$). For that position of the pole the damping ν is zero which explains the strong response by the filament to forced oscillations.

5.2. Horizontal oscillations

For horizontal oscillations we can present identical considerations. For poles on the imaginary axis ($\tilde{s} = i\tilde{\omega}$) Eq. (20) reads

$$h(i\tilde{\omega}) \;=\; -\tilde{\omega}^2 + \tilde{\Omega}_{\rm y}^2 - \frac{1}{2} - \frac{\pi}{4}\tilde{\omega}\tilde{\tau} Y_1(\tilde{\omega}\tilde{\tau}) - i\frac{\pi}{4}\tilde{\omega}\tilde{\tau} J_1(\tilde{\omega}\tilde{\tau})\;.$$

The condition $\mathrm{Im}(h(i\tilde{\omega})) = 0$ is satisfied when $\tilde{\omega}\tilde{\tau} = j_{1;{\rm k}}$ with $j_{1;{\rm k}}$ the zeros of J_1. The direction in which the poles move follows from $\mathrm{sign}(\mathrm{Re}(d\tilde{s}/d\tilde{\tau})) \sim \mathrm{sign}(J_0(j_{1;{\rm k}}))$. For $k = 0, 2, 4, \ldots$ the poles move to the right in the complex plane and for $k = 1, 3, 5, \ldots$ to the left. The expression $\mathrm{Re}(h(i\tilde{\omega})) = 0$ can be written as $\tilde{\omega}^2 = \tilde{\Omega}_{\rm y}^2 - g(j_{1;{\rm k}})$ with $g(j_{1;{\rm k}}) = \frac{1}{2}\left\{1 + \frac{\pi}{2} j_{1;{\rm k}} Y_1(j_{1;{\rm k}})\right\}$. In Table 1 we present the first six poles together with the values of $g(j_{1;{\rm k}})$. Because $0 < \tilde{\Omega}_{\rm y}^2 \lesssim 1$ we find that $\tilde{\omega}^2 = \tilde{\Omega}_{\rm y}^2 - g(j_{1;{\rm k}}) > 0$ only for $k = 0, 2, 4, \ldots$ but these poles move to the right after intersecting the imaginary axis. So for any delay time $\tau \neq 0$ there is at least one pole with $\nu > 0$ implying instability.

The above presented considerations show that, whenever delays are important, filaments in potential background fields are unstable. In vertical direction the instability sets in after the

$\mathrm{k} = 1$ pole has crossed the imaginary axis but in horizontal direction the system is unstable for any non-zero delay time.

6. Influence of Alfvén wave emission as a damping mechanism

In this section we consider the role of Alfvén wave emission by an oscillating filament as a damping mechanism. The radiative force per unit length is given by (see van den Oord & Kuperus, 1992) $F_{\rm rad} = -(I/c)^2(v/v_{\rm A})(1/d)$ with v the velocity of the filament, $v_{\rm A}$ the Alfvén velocity and d the diameter of the filament. In dimensionless units this becomes $F'_{\rm rad} = -\zeta\tau' I_0'^2 dz'/dt'$ with $\zeta \equiv z_0/(2d) \gtrsim 2$. In the dimensionless characteristic equations we therefore include a term $\zeta I_0^2 \tau s$ (we drop the accents) to account for this type of damping. Note that Alfvén wave damping does not play a role in the quasi-stationary case when the Alfvén velocity is taken to be infinite so that $F_{\rm rad} \to 0$.

6.1. Decoupled oscillations with damping

For vertical perturbations with damping, and poles on the imaginary axis, the characteristic equation is given by

$$v(i\tilde{\omega}) \;=\; -\tilde{\omega}^2 + \tilde{\Omega}_{\rm z}^2 - \frac{1}{2} + \frac{\pi}{4}\tilde{\omega}^2\tilde{\tau}^2 Y_1'(\tilde{\omega}\tilde{\tau}) + i\tilde{\omega}\tilde{\tau}\left\{\zeta + \frac{\pi}{4}\tilde{\omega}\tilde{\tau}J_1'(\tilde{\omega}\tilde{\tau})\right\} .$$

Note that the damping coefficient ζ only appears in the imaginary part of the expression. The condition $\mathrm{Im}(v) = 0$ is satisfied when $\tilde{\omega}\tilde{\tau} = 0$ or $4\zeta/\pi = -\tilde{\omega}\tilde{\tau}J_1'(\tilde{\omega}\tilde{\tau}) \equiv p(u)$ with $u \equiv \tilde{\omega}\tilde{\tau}$. The function $p(u)$ has an oscillatory behaviour around zero and the amplitude of its envelope varies proportional to $\sim \sqrt{u}$. Because $4\zeta/\pi > 0$, and because the amplitude of $p(u)$ increases while p oscillates, there exists an infinite number of solutions $u_{\rm k}$ ($\mathrm{k} = 1, 2, \ldots$) satisfying $4\zeta/\pi = p(u_{\rm k})$. When k is odd $p'(u_{\rm k}) \geq 0$ and when k is even $p'(u_{\rm k}) < 0$. The quasi-stationary pole is indicated again by $\mathrm{k} = 0$. The direction into which the poles move when they cross the imaginary axis is given by

$$\mathrm{sign}(\mathrm{Re}(\,d\tilde{s}/d\tilde{\tau}|_{u_{\rm k}})) \;\sim\; \mathrm{sign}(p'(u_{\rm k}))\,, \qquad (23)$$

$$\mathrm{sign}(\mathrm{Re}(\,d\tilde{s}/d\tilde{\tau}|_{u_0})) \;\sim\; \mathrm{sign}(-\zeta)\,. \qquad (24)$$

These expressions show that for odd k the poles move to the right and for even k, or $\mathrm{k} = 0$, to the left.

Next we have to establish for which $u_{\rm k}$ the expression $\mathrm{Re}(v) = 0$ results in $\tilde{\omega}^2 > 0$. This occurs, in fact, for $\mathrm{k} = 0$ and for odd k ($\mathrm{k} = 1, 3, 5, \ldots$) although the proof is rather lengthy. Therefore we present an approximate proof. For $u \gtrsim 2$ the Bessel functions can be approximated as $J_1' \approx \sqrt{2/\pi u}\cos\phi$ and $Y_1' \approx \sqrt{2/\pi u}\sin\phi$ with $\phi \approx u - \pi/4 + 7/8u + \ldots$. Using these approximations we can write

$$\tilde{\omega}^2 \approx \tilde{\Omega}_{\rm z}^2 - 1/2 \pm \sqrt{\pi u_{\rm k}/8}\sqrt{u_{\rm k}^2 - 16\zeta^2/\pi^2}\,,$$

where the plus sign applies for k odd and the minus sign for k even. Because $\tilde{\Omega}_{\rm z}^2 - 1/2$ varies between $\pm 1/2$ this shows that for k even, and $u_{\rm k}$ sufficiently large, $\tilde{\omega}^2$ is smaller than zero.

The following picture arises. The (quasi-stationary) pole which exists on the imaginary axis at $\tau = 0$ moves to the left when τ starts to differ from zero (Eq. (24)). The system performs damped oscillations. For larger values of $\tilde{\tau}$ other poles (those with odd k) arrive on the imaginary axis but these move to the right implying instability. We conclude that the system at $\tilde{\tau} = 0$ and at the delay time $\tilde{\tau}$ corresponding to u_1 performs undamped oscillations and at intermediate delays damped oscillations. For larger values of $\tilde{\tau}$ an increasing number of poles is found in that part of the complex plane where the system is unstable. The exact value of u_1 depends on the damping coefficient ζ. In Fig. 3a we show some trajectories of the quasi-stationary pole for different values of $\tilde{\Omega}_{\rm z}^2$. The pole is first found on the imaginary axis and then moves to the left. For larger values of $\tilde{\tau}$ it turns towards the origin.

For horizontal oscillations the following relation applies for poles on the imaginary axis

$$h(i\tilde{\omega}) \;=\; -\tilde{\omega}^2 + \tilde{\Omega}_{\rm y}^2 - \frac{1}{2} - \frac{\pi}{4}\tilde{\omega}\tilde{\tau}Y_1(\tilde{\omega}\tilde{\tau}) + i\tilde{\omega}\tilde{\tau}\left\{\zeta - \frac{\pi}{4}J_1(\tilde{\omega}\tilde{\tau})\right\} .$$

For $\tilde{\tau} > 0$ this expression can never be equal to zero because the imaginary part can never be equal to zero. In general $\zeta \gtrsim 2$ so that $4\zeta/\pi > \max(J_1) \approx 0.58$. Therefore there can only be a pole on the imaginary axis when $\tau = 0$. When τ starts to differ from zero this pole will move to the left. This follows from Eq. (24) which also applies for horizontal oscillations. This implies that, when damping is included, the system is always stable for horizontal perturbations provided the quasi-stationary system is stable. In Fig. 3b we show some trajectories of the quasi-stationary pole for different values of $\tilde{\Omega}_{\rm y}^2$. The poles are first found on the imaginary axis and move then to the right and make a loop. For larger values of $\tilde{\tau}$ they turn towards the origin. The trajectories of the poles shown in Fig. 3 depend strongly on the value of the damping coefficient ζ. To calculate the total response of the system also the poles which are not shown in the figures have to be taken into account. We note that in the case of horizontal oscillations with damping none of these poles intersects the imaginary axis. So for this case our method of integrating Eq. (21), starting on the imaginary axis, cannot be applied.

6.2. Coupled oscillations with damping

Above we showed that damping stabilizes the filament in both horizontal and vertical direction. It is interesting to see how damping affects the system in the case of coupled oscillations. For that purpose we consider a filament in an asymmetric potential background field as was discussed in Sect. 3.2. We use the expressions for the current and the frequencies as derived in that section.

In Eqs. (15) and (16) the 'coupling' terms are related according to $\partial B_{\rm y,cor}/\partial y|_{\rm E} = -\partial B_{\rm z,cor}/\partial z|_{\rm E} = kB_1$. In dimensionless units this becomes $\chi\epsilon$. The dimensionless characteristic

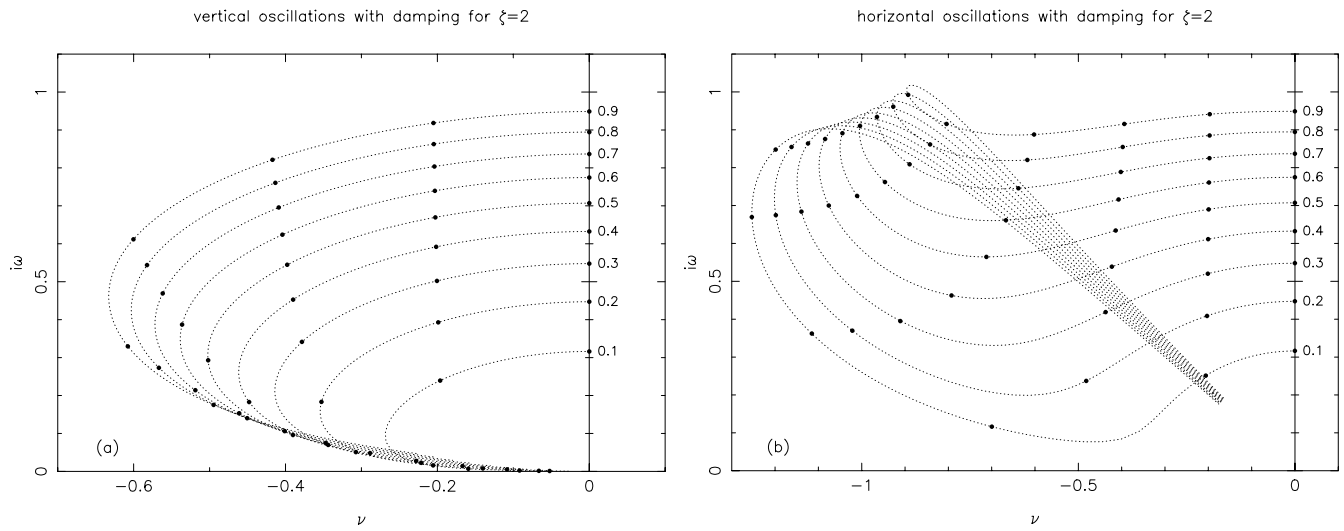

Fig. 3a and b. Behaviour of the quasi-stationary pole for a damping coefficient $\zeta = 2$. The labels indicate the values of $\tilde{\Omega}_z^2$ and $\tilde{\Omega}_y^2$. The thick dots indicate the delay times $\tilde{\tau} = 0$, 0.2, 0.4, 0.6, 0.8 and 1. Panel **a** applies to vertical oscillations. In this panel the integration was stopped at $\tilde{\tau} = 2$. For this system the k = 1 pole crosses the imaginary axis at $3.1 < \tilde{\tau} < 3.2$ for the different values of $\tilde{\Omega}_z^2$. Panel **b** applies to horizontal oscillations. The integration was stopped at $\tilde{\tau} = 10$. The scaled delay time satisfies $\tilde{\tau} = \tau' \mathrm{e}^{-\chi}$ with τ' of the order unity (Sect. 4) and $\chi < 1$. So for real filaments $\tilde{\tau} \lesssim 1$. At $\tilde{\tau} = 1$ the other poles, which are not shown, are found in the range $\tilde{\nu} < -1$, $|\tilde{\omega}| > 2.5$ for the vertical case and at $\tilde{\nu} < -1.5$, $|\tilde{\omega}| > 5$ for the horizontal case. The results depend, of course, strongly on the assumed value of ζ.

equations are given by

$$Zv(s) - YI_0\epsilon\chi = 0\,,$$
$$Yh(s) - ZI_0\epsilon\chi = 0\,,$$

where $v(s)$ and $h(s)$ now also contain the damping term $\zeta I_0^2 \tau s$. This system has only solutions when

$$\begin{vmatrix} -I_0\epsilon\chi & v \\ h & -I_0\epsilon\chi \end{vmatrix} = 0\,. \tag{25}$$

The characteristic equation for coupled oscillations is therefore given by $h(s)v(s) - I_0^2\chi^2\epsilon^2 = 0$. Note that when $\epsilon = 0$ the equations for the horizontal and vertical response decouple.

Consider first the case that delays are not important ($\tau = 0$). The characteristic equation for coupled oscillations in an asymmetric background field is given by

$$s^4 + s^2\left(\Omega_y^2 + \Omega_z^2\right) + \Omega_y^2\Omega_z^2 - I_0^2\chi^2\epsilon^2 = 0$$

so that

$$s^2 = -\frac{1}{2}\left(\Omega_y^2 + \Omega_z^2\right) \pm \frac{1}{2}\sqrt{\left(\Omega_y^2 + \Omega_z^2\right)^2 + 4I_0^2\chi^2\epsilon^2 - 4\Omega_y^2\Omega_z^2}\,.$$

For NP prominences this reads (see Sect. 3.2)

$$s^2 = \frac{1}{2}\kappa g \pm \frac{1}{2}\kappa g\left(1 + 4\frac{\chi^2}{\kappa^2\rho^2} - 4\frac{\chi}{\kappa}\right)^{1/2}\,.$$

The expression between the brackets has a minimum for $\chi/\kappa = \rho^2/2$ corresponding to $s^2 = \kappa g/2 \pm \kappa g\epsilon\exp(\chi)/2$. This implies that the 'plus-solution' always results in s^2 real and positive so that one of the roots of the quartic equation is always real and positive. We conclude that when delays are not important NP prominences in asymmetric arcades are always unstable. The reason is, of course, that the asymmetric background field we consider does not have a dip in the field lines which is required to stabilize NP filaments.

For IP prominences we find (see Sect. 3.2)

$$s^2 = -\frac{1}{2}\rho^2\mathrm{e}^{-2\chi} \pm \frac{1}{2}\rho^2\mathrm{e}^{-2\chi}\left(1 + 4\frac{\chi^2}{\rho^2} - 4\chi\right)^{1/2}$$

The behaviour of the system is determined by whether the part between the brackets is larger, equal or smaller than unity. We can distinguish three cases: 1) $\chi > \rho^2$: the plus solution results is s^2 real and positive so that one of the roots of the quartic equation is real and positive, implying instability; 2) $\chi = 0$ or $\chi = \rho^2$: the plus solution results in a pole of multiplicity 2 at the origin of the complex plane and the minus solution in two complex conjugate poles $s = \pm i\rho\exp(-\chi)$; 3) $0 < \chi < \rho^2$: both the plus and minus solution have $s^2 < 0$ so that there are four poles on the imaginary axis (pairwise complex conjugates). We conclude that without delays IP prominences in asymmetric arcades are stable provided $\chi < \rho^2$ so when $\epsilon^2 < (1-\chi)\exp(-2\chi)$.

The full characteristic equation for coupled oscillations with damping is given by

$$\tilde{s}^4 + \tilde{s}^2\left(\frac{1}{2}z^2K_2 + 2\zeta z\right) + \frac{1}{4}z^2\left(K_1^2 + zK_0K_1 - K_0\right)$$
$$+\frac{1}{2}z^2\tilde{\Omega}_y^2K_0 + \zeta z\left(\zeta z + \frac{1}{2}z^2K_2\right) - \frac{1}{4} + \tilde{\Omega}_y^2\tilde{\Omega}_z^2$$
$$+\left(\tilde{\Omega}_y^2 + \tilde{\Omega}_z^2 - 1\right)\left(\tilde{s}^2 + \zeta z + \frac{1}{2}zK_1 - \frac{1}{2}\right) = C^2$$

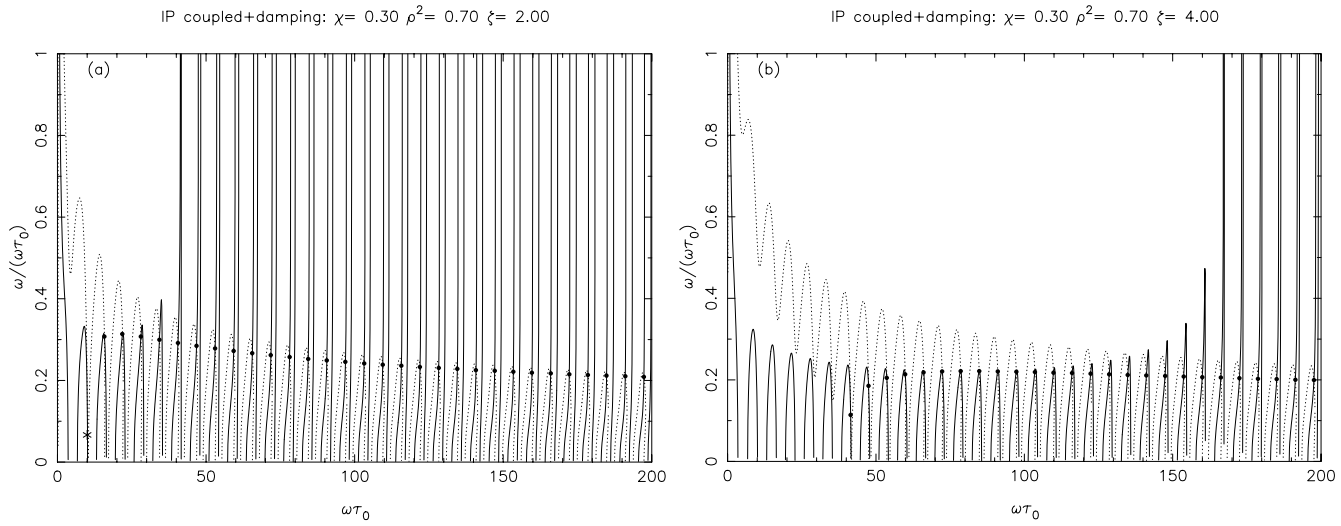

Fig. 4a and b. Solutions of Eqs. (26) (dotted lines) and (27) (solid lines) for $\zeta = 2$ (**a**) and $\zeta = 4$ (**b**). We took $\chi = 0.3$, $\rho^2 = 0.7$ so that $\epsilon = B_1/B_0 = 0.4$. Intersections of the solid and dotted lines occur at those combinations of $\tilde{\omega}$ and $\tilde{\tau}$ for which there are poles on the imaginary axis. The dots indicate the poles which result from our approximations. These approximations sometimes result in a fictitious pole, indicated by an asterisk, but in general the approximations are fairly accurate.

where $C \equiv \epsilon\chi/I_0$ is the (scaled) coupling term and $z = \tilde{s}\tilde{\tau}$. Because in a potential background field $\tilde{\Omega}_{\rm y}^2 + \tilde{\Omega}_{\rm z}^2 \approx 1$ the last term on the left-hand side can be neglected. This term does not vanish in a constant α force-free field.

The above expression is rather complicated to solve. Therefore we concentrate again on the intersections of poles with the imaginary axis. Expressing again the characteristic equation in its real and imaginary part gives

$$\mathrm{Re}(h(i\tilde{\omega})v(i\tilde{\omega}) - C^2 = 0) \;\Rightarrow\; \tilde{\omega}^4 + \tilde{\omega}^2 f_1 + f_2 = 0\,, \qquad (26)$$

$$\mathrm{Im}(h(i\tilde{\omega})v(i\tilde{\omega}) - C^2 = 0) \;\Rightarrow\; \tilde{\omega}^2 = f_3/f_4\,, \qquad (27)$$

where

$$\begin{aligned}
f_1 &= \frac{\pi}{4}u^2 Y_2\,,\\
f_2 &= \left(\frac{\pi}{4}\right)^2 u^2\left(Y_1^2 - J_1^2\right) + \left(\frac{\pi}{4}\right)^2 u^3\left(J_0 J_1 - Y_0 Y_1\right)\\
&\quad -\zeta^2 u^2 + \frac{\pi}{4}\tilde{\Omega}_{\rm y}^2 u^2 Y_0 + \frac{\pi}{4}\zeta u^3 J_2\\
&\quad -\frac{\pi}{8}u^2 Y_0 + \tilde{\Omega}_{\rm y}^2\tilde{\Omega}_{\rm z}^2 - \frac{1}{4} - C^2\,,\\
f_3 &= \frac{1}{2}\left(\frac{\pi}{2}\right)^2 u J_1 Y_1 - \left(\frac{\pi}{4}\right)^2 u^2\left(J_1 Y_0 + Y_1 J_0\right)\\
&\quad -\frac{\pi}{8}u J_0 + \frac{\pi}{4}\tilde{\Omega}_{\rm y}^2 u J_0 - \frac{\pi}{4}\zeta u^2 Y_2\,,\\
f_4 &= 2\zeta - \frac{\pi}{4}u J_2\,.
\end{aligned}$$

All Bessel functions appearing in these expressions are functions of $u = \tilde{\omega}\tilde{\tau}$. As we showed above, in the quasi-stationary limit stable coupled oscillations are only possible for IP prominences in asymmetric background fields. In Sect. 3.2 we calculated that $\tilde{\Omega}_{\rm z}^2 = 1 - \chi$, $\tilde{\Omega}_{\rm y}^2 = \chi$ while $C^2 = \chi^2(\rho^{-2} - 1)$. Stability in the quasi-stationary approach requires that $0 < \chi < \rho^2 < 1$.

In principle the equations can be solved graphically. In practice it is, however, more useful to simplify the expressions by retaining only the dominant terms. Using the fact that for large enough values of u the amplitudes of the Bessel functions vary proportional to $1/\sqrt{u}$ we find that $f_2 \to \zeta^2 u^2 - \zeta u^2 f_4$ and $f_3 \to -\zeta f_1$. With these approximations it follows that the solutions of Eqs. (26) and (27) satisfy $uJ_2(u) = 4\zeta/\pi$ and $\tilde{\omega}^2 = -(\pi/4)u^2 Y_2$. The intersections occur at those values of u for which $uJ_2(u) = 4\zeta/\pi$ and for which $Y_2(u) < 0$. In a phase/modulus representation one can write $J_2 \approx \sqrt{2/\pi u}\cos\theta$ and $Y_2 \approx \sqrt{2/\pi u}\sin\theta$ with $\theta \approx u - 5\pi/4 + 2/u - 45/128u^3 + \ldots$. The functions Y_2 and J_2 have the same amplitude and differ only in phase. For large values of u we can write $J_2(u) = 4\zeta/(\pi u) \to 0$ implying that the intersections occur at those zeros $j_{2,\rm k}$ of J_2 for which $Y_2(j_{2,\rm k}) < 0$.

In Fig. 4 we show the graphic solutions of Eqs. (26) and (27). For each of these equations we can determine $\tilde{\omega}$ as a function of $\tilde{\omega}\tilde{\tau}$. In fact, along the vertical axis we plot $1/\tilde{\tau} = \tilde{\omega}/(\tilde{\omega}\tilde{\tau})$. The dotted lines are the solutions of Eq. (26) and the solid lines of Eq. (27). Intersections of dotted and solid lines occur at those combinations of $\tilde{\omega}$ and $\tilde{\tau}$ for which there are poles on the imaginary axis. In Fig. 4a we took $\zeta = 2$ and in Fig. 4b $\zeta = 4$. The big dots are the solutions of our approximations $uJ_2 = 4\zeta/\pi$ and $\tilde{\omega}^2 = -(\pi/4)u^2 Y_2$. In general the approximation is fairly accurate although sometimes a pole is found which is not a solution of the full equations. An example of such a fictitious pole is indicated by the asterisk in Fig. 4a. Note that most of the poles intersect the imaginary axis at approximately the same time.

In the case of coupled oscillations there are two pairs of complex conjugate poles on the imaginary axis at $\tilde{\tau} = 0$. For these poles we have $\mathrm{Re}(ds/d\tilde{\tau}|_{\tilde{\tau}=0}) = -\zeta/2$ so that these poles move to the left. For the other poles it can be shown that these move to the right when they cross the imaginary axis. The sys-

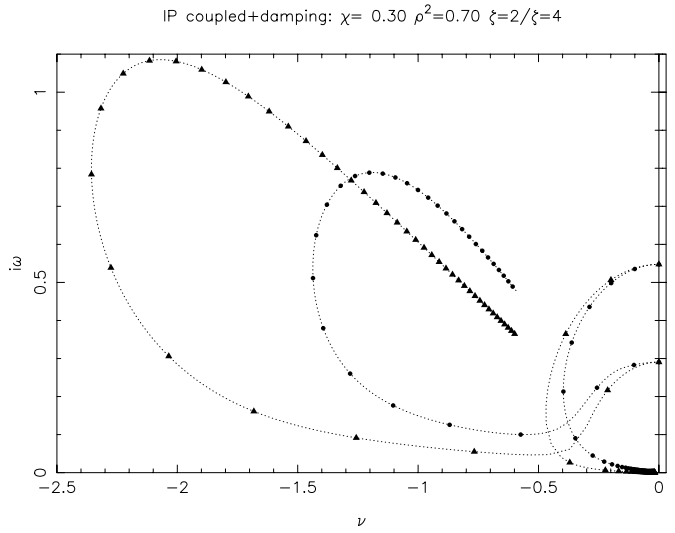

Fig. 5. Trajectories of the quasi-stationary poles for $\chi = 0.3$, $\rho^2 = 0.7$, $\zeta = 2$ (dots) and $\zeta = 4$ (triangles). The trajectories end when one of the other poles moves into the positive real half-space. For $\zeta = 2$ this occurs at $\tilde{\tau} = 3.19$ and for $\zeta = 4$ at $\tilde{\tau} = 4.52$. The increment between successive dots and triangles is $\Delta\tilde{\tau} = 0.1$.

tem performs therefore damped oscillations until the first pole crosses the imaginary axis. This is the pole with the largest value of $1/\tilde{\tau}$ in Fig. 4. In Fig. 5 we show the evolution of the two quasi-stationary poles for $\zeta = 2$ (dots) and $\zeta = 4$ (triangles). The trajectories of the poles end when the first of the other poles (not shown) moves into the positive real half-space and the system becomes unstable. The figure shows that one of the poles moves asymptotically to the origin while the other makes a loop. The size of the loop depends on the damping coefficient ζ. Note the similarities between the trajectories depicted in Fig. 3 for decoupled oscillations and those for coupled oscillations in Fig. 5.

7. Discussion and conclusions

In this paper we investigate the effect of the finite communication time between the photosphere and a filament on filament stability and possible modes of oscillation. This paper is an extension of the work by Schutgens (1997ab) in the sense that we consider both the coupled and decoupled (vertical and horizontal) response to perturbations, investigate the role of Alfvén wave damping, and put his analysis in a more general framework. When a filament is located in a symmetric coronal background field the horizontal and the vertical response are independent. In asymmetric configurations these responses are coupled. We derive the characteristic equations (Sect. 4) which depend on the delay time $\tau = 2z_0/v_{\rm A}$. In the quasi-stationary approach the Alfvén velocity is taken infinitely large (instant communication) so that $\tau = 0$. When $\tau = 0$ the (decoupled) characteristic equations reduce to the equations of the common linear stability analyses, e.g., $\delta\ddot{z} + \Omega_{\rm z}^2\delta z = 0$ and $\delta\ddot{y} + \Omega_{\rm y}^2\delta y = 0$ where $\Omega_{\rm z}$ and $\Omega_{\rm y}$ are the quasi-stationary oscillation frequencies for oscillations in the vertical and horizontal direction respectively.

It turns out that the characteristic equations can be scaled in such a way that the response of the system depends solely on the dimensionless parameters $\tilde{\Omega}_{\rm y}^2$ and $\tilde{\Omega}_{\rm z}^2$. These represent the typical ratio of the inertia of a filament oscillating with the quasi-stationary period and the Lorentz force of the photospheric current distribution (mirror current). Stability of a filament requires that both $\tilde{\Omega}_{\rm y}^2 > 0$ and $\tilde{\Omega}_{\rm z}^2 > 0$.

In Sect. 3.1 we discuss the possible range of values $\tilde{\Omega}_{\rm y}^2$ and $\tilde{\Omega}_{\rm z}^2$ can take for various types of equilibria in potential fields. We demonstrate that, within the context of line current models, Kippenhahn/Schlüter (KS) equilibria are always unstable. When the filament is located at a crest in the coronal field a KS equilibrium is horizontally unstable, as was already noticed by van Tend & Kuperus (1978), and when located at a dip it is vertically unstable. Kuperus/Raadu (KR) type equilibria are both horizontally and vertically stable when the filament is located at a crest in the coronal background field although there is a critical height at which an instability in the vertical direction sets in. For KR equilibria in potential fields we find that $\tilde{\Omega}_{\rm y}^2 + \tilde{\Omega}_{\rm z}^2 \approx 1$ so that for any stable filament $0 < \tilde{\Omega}_{\rm y}^2 < 1$ and $0 < \tilde{\Omega}_{\rm z}^2 < 1$. The fact that these parameters are in this range has important consequences for the possible range of values of the delay time τ for which a filament is stable.

We discuss so-called weak field equilibria (WF) which a characterized by a balance between the Lorentz force of the mirror current and gravity. A weak coronal field is required to provide horizontal stability. For WF equilibria $\tilde{\Omega}_{\rm y}^2 + \tilde{\Omega}_{\rm z}^2 \approx 1 - \kappa$ which is of the order unity. WF equilibria apply to very massive filaments or filaments in regions with weak coronal fields (e.g., outside active regions or near neutral lines).

In Sect. 3.4 we show that in quadrupolar coronal fields only KR and WF equilibria can exist. Depending on the height of the filament current a KR equilibrium can have an inverse or a normal polarity signature.

In Sect. 3.3 we argue that in linear force-free arcades $\tilde{\Omega}_{\rm y}^2 + \tilde{\Omega}_{\rm z}^2$ is, in principle, larger than unity, depending on the force-free parameter α. This conclusion is, however, rather academic because no realistic models exist for filaments in force-free arcades. The model by Amari & Aly (1989) places the filament between two rigid conducting vertical walls. This requires the presence of an infinite number of mirror currents in the horizontal direction to satisfy the boundary conditions at these walls. For such a system a treatment including delays is mathematically too complicated. On the other hand, one can argue that the presence of the walls stabilizes the filament in horizontal direction in an artificial way, making a stability analysis futile. In force-free arcade fields the presence of a filament generates body currents throughout the arcade so that the designation of one part of the distributed currents as the filament current is rather artificial.

In Sect. 4 we discuss the general method of solution of the characteristic equations using a simplified example. Our method of identifying the poles (zeros) of a characteristic equation differs from the method used by Schutgens (1997ab). His method is based on integration along the contour lines at which the real and the imaginary part of the characteristic equation equal zero.

This method is quite time consuming but does not require initial conditions. The method used in this paper is based on the fact that we derive the differential equation (Eq. (21)) which describes the trajectory of a pole as a function of delay time τ. By identifying the delay times at which a pole is on the imaginary axis, the location of the pole at any delay time can be found by integrating Eq. (21) using the location on the imaginary axis as initial conditions. In Sect. 5 we use this method to discuss solutions of the characteristic equations for vertical and horizontal perturbations respectively. We recover the result by Schutgens that KR equilibria respond to perturbations in the vertical direction by simple oscillations for $\tau = 0$ and $\tau = \tau_1$ and by damped oscillations for $0 < \tau < \tau_1$. Delay τ_1 is the delay time at which the first pole moves into the positive real half-space of the complex plane. We also find, however, that KR prominences are only stable to horizontal perturbations when $\tau = 0$. Any finite delay time destabilizes a filament in the horizontal direction.

Given these results we consider in Sect. 6 the effect of emission of Alfvén waves as a damping mechanism. This effect is quite pronounced. For perturbations in the horizontal direction the filament is always stable while for perturbations in the vertical direction the same picture arises as discussed above with the exception that delay time τ_1 then also depends on the damping coefficient. In Sect. 6 we also discuss the case of coupled oscillations which occur when a filament is in an asymmetric background field. Again we find that stable oscillations exist for $\tau = 0$ and for some delay time $\tau = \tau_1$, with τ_1 depending on the damping coefficient. For $0 < \tau < \tau_1$ the system performs damped oscillations. Without Alfvén wave emission the coupled system would always be unstable.

In realistic configurations the dimensionless delay time $\tilde{\tau}$ is of the order unity. Figs. 3 and 5 indicate that quality factors of the order unity can be expected. We note that observations of (damped) filament oscillations can be used as diagnostic tools. Observations of the quality factor correspond to a range of locations in the dimensionless complex ($\tilde{\nu}$,$i\tilde{\omega}$) plane, in fact, a line through the origin. By making a grid of trajectories of the poles which are on the imaginary axis at $\tau = 0$ the observed oscillation can be related to a range of dimensionless quasi-static periods $\tilde{\Omega}_{\rm y}$ or $\tilde{\Omega}_{\rm z}$ and a possible range of dimensionless delay times $\tilde{\tau}$. The combination of the observed period and the dimensionless periods gives the possible range of values the filament current I_0 can have, which, in combination with the dimensionless delay time gives the range of dimensional delay times. When the filament height is known this provides an estimate of the Alfvén speed. Because $0 < \tilde{\Omega}_{\rm y}^2 < 1$ and $0 < \tilde{\Omega}_{\rm z}^2 < 1$ the range over which I_0 and τ can vary is fairly restricted. In this way also an estimate for the damping coefficient may be obtained.

The purpose of this paper is to establish which effect delays have on the horizontal and vertical stability of filaments and their modes of oscillations. In the future the treatment can be extended by considering sound waves as a damping mechanism or by allowing different damping coefficients for horizontal and vertical perturbations. Our basic conclusion is that damping plays an important role in stabilizing filaments.

Acknowledgements. The authors acknowledge financial support from the Netherlands Organization for Scientific Research (NWO).

Appendix A: linearizing the mirror field

The expressions for the y- and the z-component of the magnetic field related to the mirror current are given in Eqs. (13) and (14). In dimensionless form these expressions read

$$B_{\rm y,mir} =$$

$$\int_0^\infty dx' \frac{2I_0}{(RF)^2}\left\{\alpha\dot{z}(t') + \frac{z(t)+z(t')}{RF}(1+\alpha^2\dot{G})\right\}$$

$$B_{\rm z,mir} =$$

$$\int_0^\infty dx' \frac{2I_0}{(RF)^2}\left\{\alpha\dot{y}(t') - \frac{y(t)-y(t')}{RF}(1+\alpha^2\dot{G})\right\}$$

with $\alpha = \tau/2$ and

$$\begin{aligned} R(t') &= \sqrt{x'^2 + (y(t)-y(t'))^2 + (z(t)+z(t'))^2} \\ &\equiv (t-t')/\alpha\,, \\ F &= 1 - \alpha\frac{(y(t)-y(t'))\dot{y}(t') - (z(t)+z(t'))\dot{z}(t')}{R}\,, \\ \dot{G} &= -\dot{y}(t')^2 + (y(t)-y(t'))\ddot{y}(t') \\ &\quad -\dot{z}(t')^2 - (z(t)+z(t'))\ddot{z}(t')\,. \end{aligned}$$

The expressions for the field components have the form

$$B = 2I_0 \times \int_0^\infty dx' K\left(z(t)+z(t'), \dot{z}(t'), \ddot{z}(t'), y(t)-y(t'), \dot{y}(t'), \ddot{y}(t')\right)$$

The integrand can be linearized around the equilibrium position according to

$$\begin{aligned} K &= K(2,0,0,0,0,0) \\ &\quad +\Delta_z \left.\frac{\partial K}{\partial z}\right|_{\rm E} + \delta\dot{z}\left.\frac{\partial K}{\partial \dot{z}}\right|_{\rm E} + \delta\ddot{z}\left.\frac{\partial K}{\partial \ddot{z}}\right|_{\rm E} \\ &\quad +\Delta_y \left.\frac{\partial K}{\partial y}\right|_{\rm E} + \delta\dot{y}\left.\frac{\partial K}{\partial \dot{y}}\right|_{\rm E} + \delta\ddot{y}\left.\frac{\partial K}{\partial \ddot{y}}\right|_{\rm E} \end{aligned}$$

where $\Delta_z \equiv \delta z(t) + \delta z(t')$ and $\Delta_y \equiv \delta y(t) - \delta y(t')$. Working out the expressions gives for the linearized field components

$$\begin{aligned} B_{\rm y,mir} &= I_0 \\ &\quad +2I_0\int_0^\infty dx' \left\{\delta z(t)\left(\frac{1}{R_0^3} - \frac{12}{R_0^5}\right)\right\}_{t'=t-\alpha R_0} \\ &\quad +2I_0\int_0^\infty dx' \left\{\delta z(t')\left(\frac{1}{R_0^3} - \frac{12}{R_0^5}\right)\right\}_{t'=t-\alpha R_0} \\ &\quad +2I_0\int_0^\infty dx' \left\{\delta \dot{z}(t')\left(\frac{\alpha}{R_0^2} - \frac{12\alpha}{R_0^4}\right)\right\}_{t'=t-\alpha R_0} \\ &\quad -2I_0\int_0^\infty dx' \left\{\delta \ddot{z}(t')\frac{4\alpha^2}{R_0^3}\right\}_{t'=t-\alpha R_0}\,, \end{aligned} \tag{A1}$$

$$B_{\rm z,mir} = -2I_0 \int_0^\infty dx' \delta y(t) \frac{1}{R_0^3} \qquad \text{(A2)}$$
$$+2I_0 \int_0^\infty dx' \left\{ \delta y(t') \frac{1}{R_0^3} + \delta \dot{y}(t') \frac{\alpha}{R_0^2} \right\}_{t'=t-\alpha R_0} ,$$

with $R_0 \equiv \sqrt{4+x'^2}$. The first term in the expression of $B_{\rm y,mir}$ (I_0) is a zero-order term which cancels with the other zero-order terms in the perturbed momentum equation. Next we Laplace transform the expressions. This is fairly simple when one uses the identity

$$\mathcal{L}\left(\int_0^\infty dx' f(t-\alpha R_0)/R_0^n \right) = \mathcal{L}\left(f(t)\right) 2^{1-n} {\rm Ki}_{n-1}(2\alpha s)$$

where ${\rm Ki}_n$ is a repeated integral of the modified Bessel function K_0 (Abramowitz & Stegun 1968). Working out the Laplace transforms using the recurrence relations for the repeated integral one finds

$$\mathcal{L}(B_{\rm y,mir}) = -(I_0/2) Z \left(1 - s^2\tau^2 K_1'(s\tau)\right) ,$$
$$\mathcal{L}(B_{\rm z,mir}) = -(I_0/2) Y \left(1 - s\tau K_1(s\tau)\right) ,$$

where $Z = \mathcal{L}(\delta z)$ and $Y = \mathcal{L}(\delta y)$.

References

Abramowitz M., Stegun I. (eds.), 1968, Handbook of Mathematical Functions, Dover Publications
Amari T., Aly J.J., 1989, A&A 208,261
Kippenhahn R., Schlüter A., 1957, Z. Astrophys. 43, 36
Kuperus M., Raadu M.A., 1974, A&A 31, 189
Schutgens N.A.J., 1997a, A&A 323, 969
Schutgens N.A.J., 1997b, A&A 325, 352
van den Oord G.H.J., Kuperus M., 1992, Solar Phys. 142,113
van Tend W., Kuperus M., 1978, Solar Phys. 59, 115